Journal of Physics D: Applied Physics

PAPER

Growth and stress analyses of vanadium dioxide nanomembranes for controllable rolling

To cite this article: Xing Li *et al* 2020 *J. Phys. D: Appl. Phys.* **53** 455105

J. Phys. D: Appl. Phys. **53** (2020) 455105 (8pp)
https://doi.org/10.1088/1361-6463/aba312

Growth and stress analyses of vanadium dioxide nanomembranes for controllable rolling

Xing Li[1], **Yang Wang**[1], **Borui Xu**[1], **Yimeng Chen**[1], **Ziao Tian**[2], **Gaoshan Huang**[1] and **Yongfeng Mei**[1]

[1] Department of Materials Science, State Key Laboratory of ASIC and Systems, Fudan University, Shanghai 200433, People's Republic of China
[2] State Key Laboratory of Functional Materials for Informatics, Shanghai Institute of Microsystem and Information Technology, Chinese Academy of Sciences, Shanghai 200050, People's Republic of China

E-mail: gshuang@fudan.edu.cn and yfm@fudan.edu.cn

Received 22 April 2020, revised 30 June 2020
Accepted for publication 6 July 2020
Published 12 August 2020

CrossMark

Abstract
Vanadium dioxide (VO_2)-based microactuators with fast and highly efficient dynamic responses have become one of the best candidates for microrobots and micromuscles. VO_2 microstructures fabricated by rolling nanomembranes with component gradient along the vertical direction are considered to be promising for future applications, and thus need further investigation. Here, we quantify the effects of substrate temperature on the initial internal stress of the nanomembranes and achieve rolled-up single-component VO_2 nanomembranes via stress engineering. Through synchrotron radiation x-ray diffraction (XRD) measurements, we find that the stress of nanomembranes is negatively correlated with substrate temperature, and its exact value can be calculated from the shift of the XRD peaks. Moreover, experimental results demonstrate that VO_2 nanomembranes deposited on a Si/SiO_2 substrate possess lower phase transition temperature and narrower hysteresis loops than those grown on quartz and Al_2O_3 substrates with similar surface morphology. The upward bending of the VO_2 nanomembrane due to the tensile stress gradient from temperature changing during deposition is demonstrated, and the rolled-up VO_2 microstructures with tunable stress and narrow hysteresis loops are considered to have advantageous applications in microactuators.

Supplementary material for this article is available online

Keywords: vanadium dioxide nanomembrane, internal stress, synchrotron radiation x-ray diffraction, microstructure

(Some figures may appear in colour only in the online journal)

1. Introduction

In recent years, VO_2 has attracted more and more attention as a kind of smart material. It is widely used in various fields due to its metal–insulator transition (MIT) at a low critical temperature (68 °C) [1]. The large changes of electrical resistance and near-infrared transmission of VO_2 over MIT are extensively applied in sensors [2], photoelectric switches [3], infrared-related devices [4] and smart windows [5]. With the development of microrobots and miromuscles actuated by external stimuli [6, 7], VO_2 is considered as one of the best candidate materials due to its large strain changes at MIT and simple triggering condition. As a foundation unit of these intelligent motion systems, microactuators with various microstructures, such as cantilevers [8], wrinkles [9] and curl [10–12] have been explored. Among various microstructures, the curl by rolling two-dimensional (2D) nanomembranes into three-dimensional (3D) microstructures demonstrates the advantages of miniaturization and great structural designability [13].

The rolled-up nanotechnology combines stress engineering and a top-down approach that achieves the precise patterning of nanomembranes, exploring the expandable and fully integrated mesoscopic structure preparation [14]. This method has strong material compatibility, including various smart materials (VO_2, Pd and so on) [15, 16]. Due to the high elastic energy density of the nanomembranes, the 3D microstructures fabricated by rolling nanomembranes have faster response speed and greater deformation under stimulation [17, 18]. Therefore, from the viewpoints of both fundamental research and practical applications, determining and regulating the initial internal stress state of the nanomembranes plays a vital role in the preparation of 3D VO_2 microstructures.

A variety of practical and reliable methods are utilized for depositing VO_2 nanomembranes, such as sputtering [19], sol–gel deposition [20] and chemical vapor deposition [21]. The magnetron sputtering becomes an outstanding method for deposition nanomembranes due to its excellent film-forming quality and high controllability of parameters [22, 23]. In the sputtering process, many parameters, including thickness, substrate temperature, oxygen–argon ratio and the target, affect the characters of the VO_2 nanomembranes [24–26]. Recent research has shown that the substrate temperature and oxygen–argon ratio in magnetron sputtering have indirect effects on the critical temperature of the MIT, because these two parameters affect the internal stress state of the VO_2 nanomembranes [27–29]. As a result, quantitative and qualitative studies on the relationship between stress and deposition parameters are of fundamental scientific significance for future applications of VO_2 nanomembranes.

In this paper, VO_2 nanomembranes grown with different parameters, e.g. substrate temperature, oxygen–argon ratio and substrates used, are tested by small-angle synchrotron radiation x-ray diffraction (XRD), a semiconductor characterization system and atomic force microscopy (AFM). The effects of these parameters on the phase transition and initial stress state of VO_2 nanomembranes are discussed in detail, which provides a good idea for the fabrication of rolled-up single-component VO_2 microstructures and Cr/VO_2 bimorph microstructures with highly controllable internal stress.

2. Experimental detail

2.1. Growth and characterization of VO_2 nanomembranes

Firstly, the SiO_2 coated Si (i.e. Si/SiO_2) substrate was cleaned by ultrasonication in acetone, ethanol and deionized water for 5 min, respectively. After cleaning, VO_2 nanomembranes were grown on Si/SiO_2 substrates by direct current magnetron sputtering of a pure V metal target. The substrate temperature (T_s) was in the range of 450 °C–550 °C, and oxygen and argon flow rates (in sccm), which can be controlled by a mass flowmeter, were set as 35:65, 40:60 or 45:55. The growth time and sputtering power during the deposition were maintained at 600 s (the thickness of VO_2 nanomembrane is about 40 nm) and 200 W, respectively. We chose fixed parameters (oxygen–argon ratio is 40:60 and T_s is 500 °C) to grow on other substrates including Al_2O_3 substrate and quartz glasses with different surface morphologies.

The VO_2 nanomembranes were characterized by small-angle synchrotron radiation XRD (Shanghai Synchrotron Radiation Facility). The angle of incidence was fixed at 0.0°, 0.4°, 0.7° and 1.0°, and the measurement was taken by using a 2θ scan configuration. The electrical properties of nanomembranes were measured on a Keithley 4200 Semiconductor Characterization System. AFM (Dimension FastScan, Bruker, Billerica, MA) was used to characterize the surface morphology of substrates and VO_2 nanomembranes.

2.2. Fabrication and characterization of single-component VO_2 and Cr/VO_2 bimorph microstructures

For single-component VO_2 microstructures, VO_2 nanomembrane was deposited on Si/SiO_2 substrate at two T_s: the lower layer was deposited at 550 °C for 300 s and the upper layer was deposited at 500 °C for 300 s. The oxygen–argon ratio and sputtering power were kept at 40:60 and 200 W, respectively. Then, a layer of photoresist (AZ-5214, Microchemicals GmbH, Germany) with about 1 μm thickness was spin-coated and etching windows (supplementary figure S1 (https://stacks.iop.org/JPD/53/455105/mmedia)) were defined by photolithography (HEIDELBERG, UPG501). After development, the window was exposed and etched by reactive ion etching (RIE) for 60 s (30 sccm CF_4 and 30 sccm Ar flow, 300 mTorr chamber pressure and 100 W etching power). For Cr/VO_2 bimorph microstructure on Si/SiO_2 substrate, the VO_2 layer was firstly deposited at 550 °C for 900 s. The etching windows were prepared in the same way as mentioned above. After patterning by photolithography, 35 nm Cr was deposited on VO_2 by electron beam deposition. After chemical removal of the photoresist layer, for the rolling process, patterned single-component VO_2 nanomembranes and Cr/VO_2 bimorphs were released from the substrate by selectively etching SiO_2 sacrificial layer by using 40% HF solution at room temperature for 5 min. Due to the high selectivity, the property of the VO_2 nanomembrane can hardly be influenced by this etching process (supplementary figure S2). Finally, critical point drying (Leica CPD030 Critical Point Dryer) was applied to dry the rolled-up VO_2 microstructures without structural collapse.

The morphological properties of these microstructures were characterized via scanning electron microscopy (SEM, JEOL JSM-6701 F).

3. Results and discussion

For 3D VO_2 microstructures with potential applications in the field of microactuators, it is important to prepare high-quality VO_2 nanomembranes with tunable and controllable properties. In our experiment, we have prepared eight VO_2 samples by magnetron sputtering on different substrates, which are named as S1–S8. The detailed deposition parameters of VO_2 nanomembrane samples are listed in table 1 and corresponding small-angle synchrotron radiation XRD patterns of samples S1–S5 on Si/SiO_2 substrates are shown in figure 1(a).

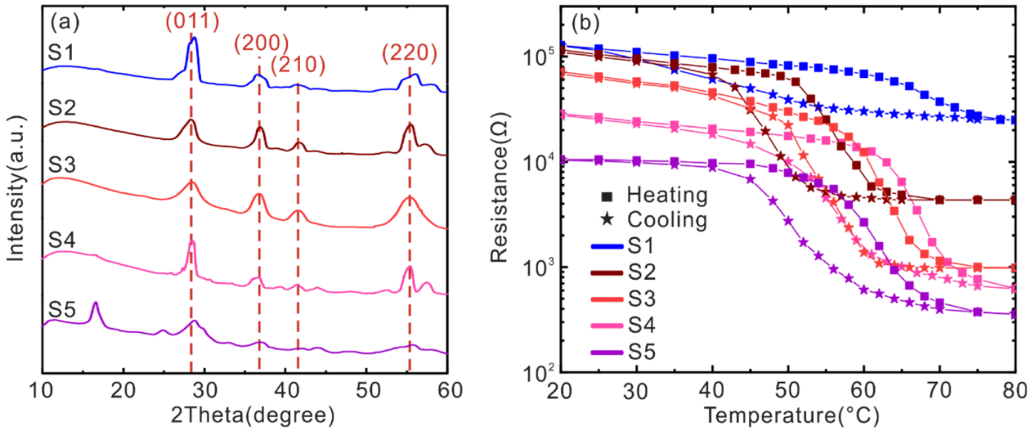

Figure 1. (a) The small-angle (0.4°) synchrotron radiation XRD patterns of S1-S5. (b) Temperature-dependent resistances (R–T curves) of S1-S5 with MIT.

Table 1. Deposition parameters of VO_2 nanomembrane samples. T_s represents the substrate temperature.

Sample	O_2 flow (sccm)	Ar flow (sccm)	T_s (°C)	Substrate
S1	35	65	450	Si/SiO_2
S2	40	60	450	Si/SiO_2
S3	40	60	500	Si/SiO_2
S4	40	60	550	Si/SiO_2
S5	45	55	500	Si/SiO_2
S6	40	60	500	quartz-2
S7	40	60	500	quartz-1
S8	40	60	500	Al_2O_3

Table 2. XRD peak positions of VO_2 nanomembrane samples.

Sample	VO_2 (011)	VO_2 (200)	VO_2 (210)	VO_2 (220)
PDF#44-0252	27.860	36.920	42.240	55.540
S1	28.79	36.58	41.41	56.11
S2	28.43	36.54	41.40	55.38
S3	28.47	36.76	41.64	55.41
S4	28.55	36.91	41.80	55.51
S5	28.79	37.06	41.93	55.77

Table 3. The contribution of different orientations to the stress of sample S3.

Spacings	K (GPa)	M	σ_φ (GPa)	$P(k\ l\ m)$
(0 1 1)	−1.7388	−0.1130	0.1964	32.64%
(2 0 0)	−1.2248	−0.1206	0.1477	23.83%
(2 1 0)	−1.0174	−0.1516	0.1542	20.21%
(2 2 0)	−0.6364	−0.1725	0.1097	23.32%

According to our XRD results, the nanomembranes grown with different experimental parameters display four characteristic peaks commonly seen in VO_2 (M), which correspond to lattice planes of (011), (200), (210) and (220), respectively. When the substrate temperature is over 500 °C (i.e. S4) or oxygen–argon ratio is greater than 40:60 (i.e. S5), some peaks from high-valence vanadium oxide appear at 16.9° and 24.7°, indicating that the VO_2 nanomembranes are further oxidized at high temperatures and in an oxygen-rich atmosphere. The positions of the four characteristic peaks of S1-S5 are summarized in table 2. The XRD reference data of VO_2 (PDF#44-0252) are listed in table 2 for comparison. Here, the peak shifts (Δd) between VO_2 samples and reference data of VO_2 are calculated and summarized in supplementary table S1. For samples S3, S4 and S5, which are both deposited with the same oxygen and argon flow rates, we can see that $\Delta d(011)$ increases with increasing T_s, but Δd of other lattice planes decreases with increasing T_s. These results indicate that the stress in the nanomembrane is anisotropic. However, we notice that the influence from the oxygen–argon ratio is relatively irregular. Therefore, our XRD results suggest that the internal stress in VO_2 nanomembranes is mainly influenced by the substrate temperature. The variation of oxygen–argon ratio affects the composition, oxygen vacancy and defect of VO_2 nanomembranes simultaneously [23], leading to a complex situation, and as a result, it is difficult to establish a qualitative relationship between oxygen–argon ratio and internal stress of nanomembranes.

The measurement results of temperature-dependent resistances (i.e. R–T curves) of S1–S5 are shown in figure 1(b). According to the results, the smallest resistance change during MIT can be observed in sample S1, and the magnitude change of this transition increases with increasing oxygen–argon ratio or rising T_s. It has been previously reported in the literature that the phase transition temperature is affected by multiple factors that are film composition, stoichiometry and stress [27, 29]. Here, the sample S1 deposited with oxygen–argon ratio of 35:65 has the highest phase transition temperature (68.1 °C) and the phase transition temperature of sample S5 deposited with oxygen–argon ratio of 45:55 is 61.8 °C. Samples S3, S4 and S5 grown with the same oxygen–argon ratio of 40:60, and the corresponding phase transition temperatures are 57.1, 63.9 and 66.2 °C respectively, demonstrating positive correlation between the substrate temperature during deposition and the phase transition temperature. However, the influence of the oxygen atmosphere during sputtering on the characters of VO_2 nanomembranes is multifaceted [25]. It is difficult to establish a direct relationship between the phase transition temperature and the oxygen flow concentration. Therefore, altering the substrate temperature is considered to be appropriate to experimentally regulate internal stress and phase transition temperature of the sputtering-produced nanomembranes.

It is well known that the substrate should also influence the feature of the nanomembrane remarkably [30]. In addition, the selection of substrate is also a key factor in the fabrication of 3D microstructures by wet chemistry-based rolled-up nanotechnology [31]. For the purpose of the nanomembrane releasing, it is necessary that the surface layer of the substrate or the sacrificial layer should react with an etching solution while the top functional layer should not. Therefore, oxide substrates with sufficiently smooth surface, such as transparent quartz, Al_2O_3 and Si/SiO_2 substrates, have been selected in our experiment. The average surface roughnesses of quartz-1, quartz-2, Al_2O_3 and Si/SiO_2 are 1.31, 5.48, 0.456 and 0.154 nm, respectively (please see also supplementary figure S3). We then carefully studied the influence of these substrates on VO_2 nanomembrane growth. As shown in figures 2(a)–(d), the surface morphologies of VO_2 nanomembranes on corresponding substrates demonstrate average surface roughness of 1.29, 8.91, 1.70 and 4.70 nm. Compared with the VO_2 nanomembranes on Si/SiO_2 substrate, the nanomembranes deposited on quartz and Al_2O_3 substrates have lower surface roughness. The R-T curves of VO_2 nanomembranes on different substrates are shown in figure 2(e). The VO_2 nanomembranes grown on quartz-2 (S6) show a linear plot in the R-T curve, indicating that the crystal structure of S6 is VO_2 (B) (please see also supplementary figure S4). On the other hand, samples S3, S7 and S8 demonstrate obvious MIT. The phase transition temperatures of S7 and S8 are 65.2 and 65.9 °C, respectively. The changes of resistance during MIT in S7 and S8 are less than 2 orders of magnitude and the phase transition hysteresis width was larger than S1–S5 grown on Si/SiO_2 substrate. Therefore, the quality and property of VO_2 nanomembranes are greatly affected by the substrate used, and the surface roughness of the substrate might influence the nanomembrane growth. In addition, substrate effects on transition temperature of the above nanomembranes have been previously confirmed and were ascribed to thermal expansion mismatch between the nanomembrane and the substrate [32–35]. Thus, in the present work, VO_2 nanomembranes grown on substrates with large thermal expansion coefficients demonstrate lower phase transition temperatures. The VO_2 nanomembranes deposited on Si/SiO_2 and quartz substrate can be better applied in the field of actuator, because the VO_2 nanomembrane on these substrates possess low critical temperature and narrow hysteresis width (see figures 1(b) and 2(e)).

As mentioned earlier, if the initial internal stress of the VO_2 nanomembranes deposited with different parameters can be calculated quantitatively, it will guide the realization of rolled-up single-component VO_2 nanomembranes without introducing other materials as a stress layer. Figures 3(a) and (f) show the XRD patterns of VO_2 nanomembranes that were measured by small-angle synchrotron radiation XRD with

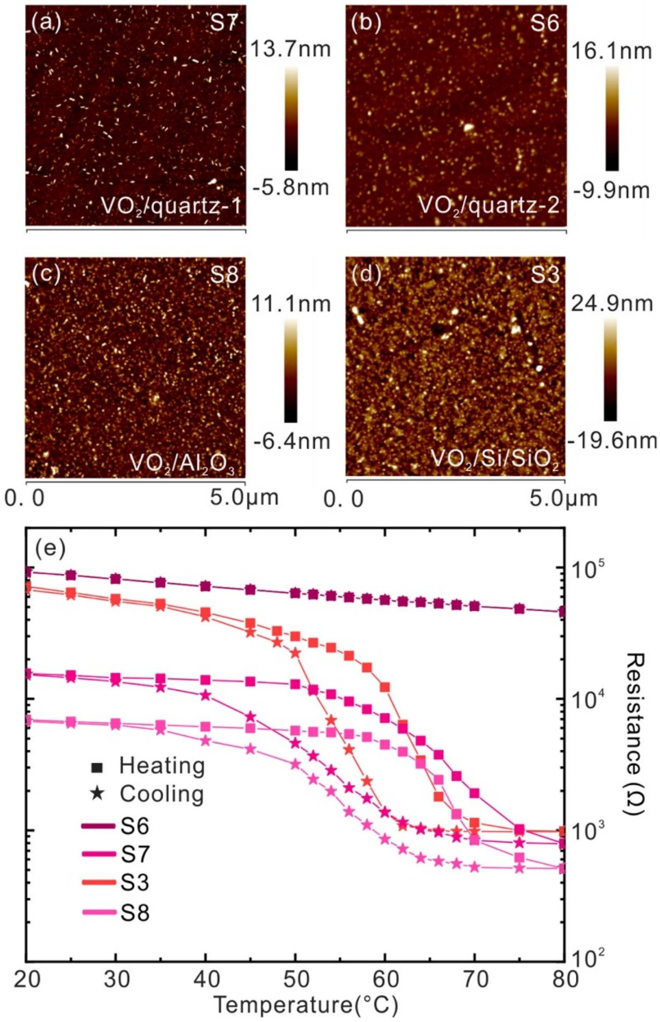

Figure 2. (a)–(d) AFM images of VO_2 nanomembranes deposited on different substrates. (e) Temperature-dependent resistance (R–T curves) of VO_2 nanomembranes on different substrates. During deposition, the oxygen–argon ratio is 40:60 and T_s is 500 °C.

different incidence angles (ψ). It shows that the peak position of VO_2 shifts to a smaller angle with increasing ψ. So, the stress state of the nanomembrane can be accurately calculated by a series of formulae (the detailed calculations can be found in the supplementary note 1) [36]. The residual stress σ_φ in the nanomembrane is

$$\sigma_\varphi = -\frac{E}{2(1+\nu)} cot\theta_0 \frac{\pi}{180} \frac{\partial(2\theta)}{\partial(sin^2\psi)}, \quad (1)$$

where σ_φ is the stress of a certain crystal orientation (φ) at different ψ, ν is the Poisson ratio, E is the Young's modulus of the VO_2 (~140 GPa) and θ is the Bragg angle.

For the sake of clarity, here we define

$$K = -\frac{E}{2(1+\nu)} cot\theta_0, \quad (2)$$

and

$$M = \frac{\partial(2\theta)}{\partial(sin^2\psi)}. \quad (3)$$

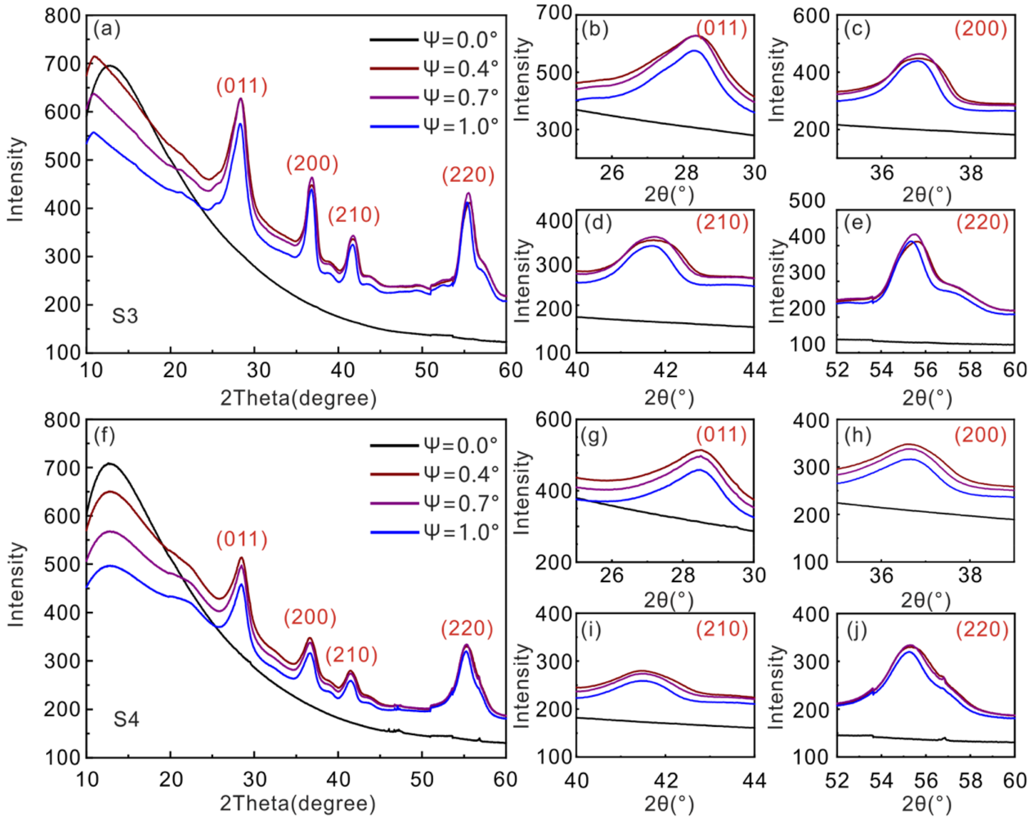

Figure 3. (a) XRD patterns of sample S3 that were measured by small-angle synchrotron radiation XRD with different incidence angles (ψ). (b)–(e) Corresponding enlarged spectra show individual VO_2 peaks. (f) XRD patterns of sample S4 that were measured by small-angle synchrotron radiation XRD with different incidence angles (ψ). (g)–(j) Corresponding enlarged spectra show individual VO_2 peaks.

Thus we obtain

$$\sigma_\varphi = K \times M. \tag{4}$$

The XRD scans of polycrystalline VO_2 nanomembranes show the contribution of several orientations, namely (011), (200), (210) and (220). The relative domain population corresponding to the ($k\ l\ m$)-oriented area, which represents the concentration of different orientations, can be represented as follows [37]:

$$P_{(k\,l\,m)} = \frac{I(k\,l\,m)}{(I(0\,1\,1) + I(2\,0\,0) + I(2\,1\,0) + I(2\,2\,0))}, \tag{5}$$

where I ($k\ l\ m$) represents the XRD intensity of the ($k\ l\ m$) reflection. The domain population $P_{(k\,l\,m)}$ corresponding to the (011), (200), (210), and (220) oriented areas can therefore be determined by XRD diagrams.

Average stress σ in the nanomembrane can thus be calculated by

$$\sigma = \sum_{i=1}^{4} P_{(k\,l\,m)} \sigma_\varphi^{(k\,l\,m)}(x). \tag{6}$$

Thus, we propose an approach to determine the residual stress in VO_2 nanomembranes with the help of XRD characterization, and the influence from the substrate temperature can be investigated. On the basis of the XRD results shown in figure 3, the calculated stress statuses are given in tables 3 and 4. The average internal stresses σ of VO_2 nanomembranes are calculated to be 0.1561 GPa in sample S3 deposited at 500 °C and 0.1321 GPa in sample S4 deposited at 550 °C, indicating the tensile stress in VO_2 nanomembrane decreases with increasing T_s. In addition, tables 3 and 4 demonstrate that VO_2 nanomembranes have the largest tensile stress in the (011) direction and the smallest tensile stress in the (220) direction. Therefore, our results prove that the stress should originate from the mismatch of lattice and thermal expansion in the VO_2 nanomembrane [38]. It is worth noting that the calculation of the exact value of internal stress in the nanomembrane should be very helpful in tuning deposition parameters for fabricating stress-driven self-assembled microstructures.

As we have discussed, small internal tensile stress exists in VO_2 nanomembranes deposited at 500 °C and relatively large stress exists in VO_2 nanomembranes deposited at 550 °C.

Table 4. The contribution of different orientations to the stress of sample S4.

Spacings	K (GPa)	M	σ_φ (GPa)	$P(k\,l\,m)$
(0 1 1)	−1.7388	−0.0981	0.1706	30.29%
(2 0 0)	−1.2248	−0.1021	0.1251	24.68%
(2 1 0)	−1.0174	−0.1323	0.1346	18.83%
(2 2 0)	−0.6364	−0.1451	0.0923	26.20%

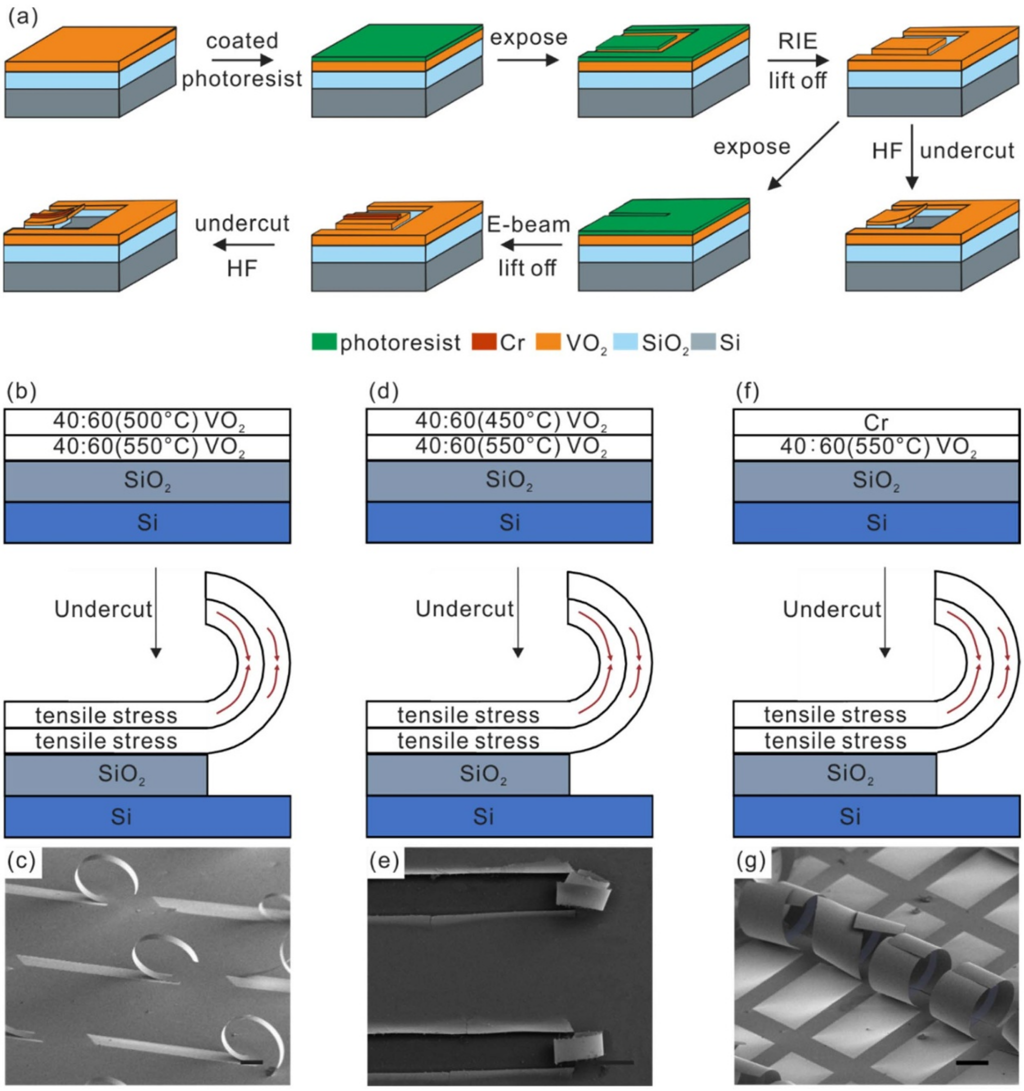

Figure 4. (a) The schematic of the fabrication process of rolled microstructures. (b) (d) and (f) are the schematic representations of the sample structure and the rolling process of single-component VO_2 nanomembranes (panels (b) and (d)) and Cr/VO_2 bimorph (f). The red arrows qualitatively represent the contraction after the tensiled layers are released. The values represent the oxygen–argon ratio and T_s. (c) and (e) SEM images of rolled-up VO_2 microstructures with different curvatures. (g) SEM image of rolled-up Cr/VO_2 microstructures. Scale bars in panels (c), (e) and (g): 100 μm.

According to these results, we can design and fabricate microstructures by rolling nanomembranes, as schematically shown in figure 4(a). To introduce the necessary stress gradient for a rolling process [17], we deposit VO_2 nanomembranes at two different substrate temperatures in one sputtering experiment, and the corresponding schematic of a nanomembrane consisting of two layers of VO_2 is shown in figure 4(b). Here, the two layers deposited at 550 and 500 °C respectively are in tensile status with different values. When the nanomembrane with the vertical stress gradient is released from the substrate, the larger contraction of the upper part of the nanomembrane compared to the lower part creates a net bending force with the direction away from the substrate [39]. Figure 4(c) shows the obtained microring by rolling VO_2 nanomembranes. The radius of the microring is about ~121 μm, which agrees with the theoretical estimation by the formula [29]:

$$\Delta\sigma = \Delta\varepsilon \times E, \tag{7}$$

$$R = \frac{(t_{upper} + t_{lower})^3}{6\Delta\varepsilon\,(1+v)\,t_{upper}t_{lower}}, \tag{8}$$

where strain difference $\Delta\varepsilon = \Delta\sigma/E = 0.024GPa/E$ and t_{upper} and t_{lower} are thicknesses of the two layers which are both 20 nm in our experiment.

In order to further demonstrate the controllability of the current approach, we prepared two more samples by manipulating the stress gradient in the nanomembranes. As shown in figure 4(d), the two VO_2 layers in the first sample were deposited at 550 and 450 °C respectively. The obtained microring (figure 4(e)) possesses a reduced diameter of ~92 μm, indicating the increased vertical stress gradient, while for the second sample, the two layers were deposited at 500 and 550 °C respectively (supplementary figure S5(a). Note the reversed layer order and downward rolling behaviour is observed (supplementary figure S5(b)). We also prepared a Cr/VO_2 bilayer nanomembrane where the Cr layers are remarkably tensiled (0.1% tensile strain), as shown in figure 4(f). Tubular structure by rolling a Cr/VO_2 bimorph is shown in figure 4(g) and the radius is about ~101 μm. Our experimental results indicate that the current approach of generating a controlled stress gradient in nanomembrane for rolling is reliable. In addition, the curvature of the rolled microstructure could be tuned in a large range, and the rolling direction could be changed because the required stress gradient is produced by two stressing layers. The current experimental approach demonstrates good controllability in producing rolled microstructures.

4. Conclusion

In summary, we studied the influences of oxygen–argon ratio, substrate temperature and substrate on the properties of the VO_2 nanomembranes prepared by magnetron sputtering. It can be found that the internal tensile stress is reduced with the increasing substrate temperature. With the substrate temperature increasing from 450 to 550 °C, the phase transition temperature of the VO_2 nanomembrane rises up from 57.1 to 66.2 °C, and the increase of oxygen–argon ratio leads to decreased resistance after MIT. Besides this, we found that VO_2 nanomembranes deposited on Si/SiO_2 substrates possess lower phase transition temperature and narrower hysteresis loop. Moreover, the stresses in the nanomembranes are calculated in detail with the help of XRD patterns, and by using these calculation results, VO_2 rolled microstructures with different rolling directions and curvatures are designed and fabricated via stress engineering. Rolled-up VO_2 nanomembranes with regulable stress can be promising in micromanipulation, optomechanical, microrobots, heat regulation and artificial muscle.

Acknowledgments

This work is supported by the Natural Science Foundation of China (Nos. U1632115, 51961145108 and 61975035), Science and Technology Commission of Shanghai Municipality (Nos. 19XD1400600 and 17JC1401700). The authors would like to thank the Shanghai Synchrotron Radiation Facility BL15U1 and its staff Ling Zhang for allowing us to perform the XRD analyses. Part of the experimental work was carried out in Fudan Nanofabrication Laboratory and Shanghai Institute of Microsystem and Information Technology, CAS.

ORCID iDs

Gaoshan Huang https://orcid.org/0000-0002-0525-7177
Yongfeng Mei https://orcid.org/0000-0002-3314-6108

References

[1] Golan G, Axelevitch A, Sigalov B and Gorenstein B 2003 Metal-insulator phase transition in vanadium oxides films *Microelectron. J.* **34** 255–8

[2] Kim B, Lee Y W, Chae B, Yun S J, Oh S, Kim H and Lim Y 2007 Temperature dependence of Mott transition in VO_2 and programmable critical temperature sensor *Appl. Phys. Lett.* **90** 023515

[3] Liu M *et al* 2007 Terahertz-field-induced insulator-to-metal transition in vanadium dioxide metamaterial *Nature* **487** 345–8

[4] Kats M A, Blanchard R, Zhang S, Genevet P, Ko C, Ramanathan S and Capasso F 2013 Vanadium dioxide as a natural disordered metamaterial: perfect thermal emission and large broadband negative differential thermal emittance *Phys. Rev.* X **3** 041004

[5] Ke Y, Zhou C, Zhou Y, Wang S, Chan H S and Long Y 2018 emerging thermal-responsive materials and integrated techniques targeting the energy-efficient smart window application *Adv. Funct. Mater.* **28** 1800113

[6] Chen P, Xu Y, He S, Sun X, Pan S, Deng J, Chen D and Peng H 2015 Hierarchically arranged helical fibre actuators driven by solvents and vapours *Nat. Nanotechnol.* **10** 1077–83

[7] Lima M D *et al* 2012 Electrically, chemically, and photonically powered torsional and tensile actuation of hybrid carbon nanotube yarn muscles *Science* **338** 928–32

[8] Wang T, Torres D, Fernández F E, Green A J, Wang C and Sepúlveda N 2015 Increasing efficiency, speed, and responsivity of vanadium dioxide based photothermally driven actuators using single-wall carbon nanotube thin-films *ACS Nano* **9** 4371–8

[9] Manca N, Pellegrino L, Kanki T, Venstra W J, Mattoni G, Higuchi Y, Tanaka H, Caviglia A D and Marre D 2017 Selective high-frequency mechanical actuation driven by the VO_2 electronic instability *Adv. Mater.* **29** 1701618

[10] Liu K, Cheng C, Suh J, Tang-Kong R, Fu D, Lee S, Zhou J, Chua L O and Wu J 2013 Powerful, multifunctional torsional micromuscles activated by phase transition *Adv. Mater.* **26** 1746

[11] Ma H, Hou J, Wang X, Zhang J, Yuan Z, Xiao L, Wei Y, Fan S, Jiang K and Liu K 2016 Flexible, all-inorganic actuators based on vanadium dioxide and carbon nanotube bimorphs *Nano Lett.* **17** 421–8

[12] Tian Z, Xu B, Hsu B, Stan L, Yang Z and Mei Y 2018 Reconfigurable vanadium dioxide nanomembranes and microtubes with controllable phase transition temperatures *Nano Lett.* **18** 3017–23

[13] Tian Z, Huang W, Xu B, Li X and Mei Y 2018 Anisotropic rolling and controlled chirality of nanocrystalline diamond nanomembranes toward biomimetic helical frameworks *Nano Lett.* **18** 3688–94

[14] Rogers J, Huang Y, Schmidt O G and Gracias D H 2016 Origami MEMS and NEMS *MRS Bull.* **41** 123–9

[15] Li X, Wang Y, Xu B, Zhou X, Men C, Tian Z and Mei Y 2019 Rolled-up single-layered vanadium oxide nanomembranes for microactuators with tunable active temperature *Nanotechnology* **30** 354003

[16] Xu B, Tian Z, Wang J, Han T, Lee T and Mei Y 2018 Stimuli-responsive and on-chip nanomembrane micro-rolls for enhanced macroscopic visual hydrogen detection *Sci. Adv.* **4** eaap8203

[17] Wang Y, Li X, Xu B, Tian Z, Di Z and Mei Y 2019 Rolling origami with smart materials *Sci. Bull.* **64** 1080–2

[18] Ning X, Wang X, Zhang Y, Yu X, Choi D, Zheng N, Kim D, Huang Y, Zhang Y and Rogers J A 2018 Assembly of advanced materials into 3D functional structures by methods inspired by origami and kirigami: a review *Adv. Mater. Interfaces* **5** 1800284

[19] Brassard D, Fourmaux S, Jean-Jacques M, Kieffer J C and Khakani M A E 2005 Grain size effect on the semiconductor-metal phase transition characteristics of magnetron-sputtered VO_2 thin films *Appl. Phys. Lett.* **87** 051910

[20] Chae B, Kim H, Yun S, Kim B, Lee Y, Youn D and Kang K 2006 Highly oriented VO_2 thin films prepared by sol-gel deposition method *Electrochem. Solid-State Lett.* **9** C12

[21] Manning T D, Parkin I P, Pemble M E, Sheel D and Vernardou D 2004 Intelligent window coatings: atmospheric pressure chemical vapor deposition of tungsten-doped vanadium dioxide *Chem. Mater.* **9** 744–9

[22] Yamin T, Wissberg S, Cohen H, Cohen-Taguri G and Sharoni A 2016 Ultrathin films of VO_2 on r-cut sapphire achieved by postdeposition etching *ACS Appl. Mater. Interfaces* **8** 14863–70

[23] Cui H, Teixeira V, Meng L, Wang R, Gao J and Fortunato E 2008 Thermochromic properties of vanadium oxide films prepared by dc reactive magnetron sputtering *Thin Solid Films* **516** 1484–8

[24] Meng Y, Huang K, Tang Z, Xu X, Tan Z, Liu Q, Wang C, Wu B, Wang C and Cao J 2018 The effect of argon pressure dependent V thin film on the phase transition process of (020) VO_2 thin film *Appl. Surf. Sci.* **427** 304–11

[25] Yu Q, Li W, Liang J, Duan Z, Hu Z, Liu J, Chen H and Chu J 2013 Oxygen pressure manipulations on the metal-insulator transition characteristics of highly (0 1 1)-oriented vanadium dioxide films grown by magnetron sputtering *J. Phys. D: Appl. Phys.* **46** 055310

[26] Castro M S, Ferreira C L and Avillez R R 2013 Vanadium oxide thin films produced by magnetron sputtering from a V_2O_5 target at room temperature *Infrared Phys. Technol.* **60** 103–7

[27] Chen Y*et al* 2017 Pressure-temperature phase diagram of vanadium dioxide *Nano Lett.* **17** 2512–6

[28] Matsuoka K, Okimura K, Azhan N H and Zaghrioui M 2019 Persistent M2 phase in strongly strained (011)-oriented grains in VO_2 films grown on sapphire (001) in reactive sputtering *J. Appl. Phys.* **125** 165304–7

[29] Yang Y, Mao X, Yao Y, Huang H, Lu Y, Luo L, Zhang X, Yin G, Yang T and Gao X 2019 Thickness effects on the epitaxial strain states and phase transformations in (001)-VO_2/TiO_2 thin films *J. Appl. Phys.* **125** 082508

[30] Mei Y, Huang G, Solovev A A, Ureña E B, Monch I, Ding F, Reindl T, Fu R K Y, Chu P K and Schmidt O G 2008 Versatile approach for integrative and functionalized tubes by strain engineering of nanomembranes on polymers *Adv. Mater.* **20** 4085–90

[31] Grimm D, Bufon C C B, Deneke C, Atkinson P, Thurmer D J, Schäffel F, Gorantla S, Bachmatiuk A and Schmidt O G 2012 Rolled-up nanomembranes as compact 3D architectures for field effect transistors and fluidic sensing applications *Nano Lett.* **13** 213–8

[32] Zhao Y, Chen C, Pan X, Zhu Y, Holtz M, Bernussi A and Fan Z 2013 Tuning the properties of VO_2 thin films through growth temperature for infrared and terahertz modulation applications *J. Appl. Phys.* **114** 113509

[33] Ufert K D 1976 Stress induced switching in VO_2 thin films *Phys. Status Solidi* a **34** K83

[34] Case F C 1984 Modifications in the phase transition properties of predeposited VO_2 films *J. Vac. Sci. Technol.* A **2** 1509

[35] Sakai J, Zaghrioui M, Matsushima M, Funakubo H and Okimura K 2014 Impact of thermal expansion of substrates on phase transition temperature of VO_2 films *J. Appl. Phys.* **116** 123510

[36] Zheng X, Li J and Zhou Y 2004 X-ray diffraction measurement of residual stress in PZT thin films prepared by pulsed laser deposition *Acta Mater.* **52** 3313–22

[37] Sakashita Y, Ono T, Segawa H, Tominaga K and Okada M 1991 Preparation and electrical properties of MOCVD-deposited PZT thin films *J. Appl. Phys.* **69** 8352

[38] Freund L 2000 Substrate curvature due to thin film mismatch strain in the nonlinear deformation range *J. Mech. Phys. Solids* **48** 1159–74

[39] Songmuang R, Deneke C and Schmidt O G 2006 Rolled-up micro- and nanotubes from single-material thin films *Appl. Phys. Lett.* **89** 223109